(Preprint) AAS 21-667

TRAJECTORY DESIGN AND ORBIT DETERMINATION OF HERA'S MILANI CUBESAT

C. Bottiglieri[*], F. Piccolo[*], A. Rizza[*], C. Giordano[*], M. Pugliatti[*], V. Franzese[*], F. Ferrari[*], and F. Topputo[*]

Hera is the European contribution to the ESA-NASA collaboration AIDA. During the mission, two CubeSats will be released in proximity of the binary asteroid 65803-Didymos: Milani and Juventas. In this work, some challenging aspects of the mission analysis of Milani are presented. Original trajectory design solutions are devised as a response to demanding scientific and operational requirements in a low-gravity environment. Then, a navigation strategy based on a combination of radiometric and optical measurements is presented and results of the knowledge analysis are shown for the main phases of the mission.

INTRODUCTION

In 2027, Hera will rendezvous with the binary asteroid 65803 Didymos as the European contribution to AIDA (Asteroid Impact and Deflection Assessment).[1] AIDA is an international collaboration between ESA and NASA, who is responsible for the Double Asteroid Redirection Test (DART)[2] kinetic impactor spacecraft. Hera and DART have been conceived to be mutually independent, however their value is increased when combined. Indeed, Hera is a planetary defense mission aimed to investigate the effect of DART impact, with scientific objectives achievable as by-product.
In proximity of the target, Hera will release two 6U CubeSat: Milani[3] and Juventas.[4] The two nanosatellites will be the first CubeSats to orbit in the close proximity of a small body and the first to perform scientific and technological operations around a binary asteroid. Politecnico di Milano is responsible for the mission design and analysis as well as for the design and analysis of Milani's GNC subsystem.
This work is focused on Milani's mission analysis, and in particular on its trajectory design and navigation strategy. First, some information on the asteroid and the reference frame used will be presented. Then, the dynamical environment of the system will be shown together with the equation of motion for the CubeSat. Following this, a detailed discussion on Milani's trajectory solutions to the most challenging scientific goals of the mission. Particular attention will be given to close proximity operations due to the highly challenging scientific and operational constraints. Finally, Milani's navigation strategy will be presented as a combination of radiometric and optical measurements.

Didymos Properties

Didymos is a binary Near-Earth Asteroid (NEA) of S-type discovered in 1996 formed by Didymos, or D1 (the primary) and Dimorphos, or D2 (the secondary). Up-to-date data about Didymos

[*]Department of Aerospace Science and Technology, Politecnico di Milano, Via La Masa 34, 20156, Milano, Italy. E-mail: claudio.bottiglieri@polimi.it, telephone: +39 02 2399 7158

and Dimorphos are reported in Table 1.

Table 1. (Top) Binary system parameters (semi-major axis, eccentricity, inclination, revolution period). (Bottom) Didymos and Dimorphos mass and spin periods properties as in Naidu et al.[5]

System Parameters			
a	**e**	**i**	**T**
1.66446 AU	0.3839	3.4083°	770 days
Asteroids Parameters			
$\mathbf{M_1}$	$\mathbf{M_2}$	$\mathbf{T_1}$	$\mathbf{T_2}$
5.226×10^{11} kg	4.860×10^{9} kg	2.26h	11.92h

The orbital properties are retrieved from the up-to-date kernels of the Hera mission*. In the up-to-date reference model, two assumptions have been made on the mutual orientation of the asteroids. Dimorphos' orbital and rotational angular momentum and Didymos' spin vector are assumed aligned, and Dimorphos' spin period and revolution period are assumed synchronized. The first implies that Dimorphos and Didymos share the same equatorial plane on which their relative motion occours; the latter means that Dimorphos is in a tidally locked configuration with Didymos. This can be relevant when observing some features on the secondary, like the DART crater. Indeed, the crater would always be in the same relative position with respect to the barycenter at each orbital period of D2 around D1. In this work, two reference frames have been used. A quasi-inertial frame called "DidymosEclipJ2000" which is centered in the system barycenter and has the xy plane on the ecliptic at the epoch J2000 and the z-axis orthogonal to that plane. The axis are inertially fixed and the system can be considered inertial for intervals of time negligible with respect to Didymos' heliocentric motion. The other is a non-inertial reference frame in which some results are shown. This frame has its xy plane on the equator of D1, with the x-axis aligned to the projection of the Sun vector on the equator and the z-axis aligned to the south pole of Didymos. This frame is also centered in the system barycenter and it is called "DidymosEquatorialSunSouth"(see Figure 1).

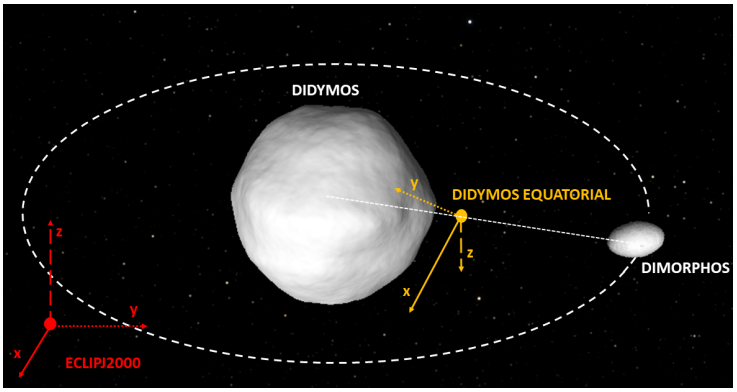

Figure 1. Didymos geometry. The reference frames are higlighted. The red frame is the inertial Eclip2000 which corresponds to the quasi-inertial DidymosEclipJ2000 when centered in the system barycenter. The yellow frame is the DidymosEquatorialSunSouth.

*https://www.cosmos.esa.int/web/spice/data Version 1.0 24/03/21

DYNAMICAL ENVIRONMENT

The dynamics of Milani in the proximity of the binary asteroid are modeled using the perturbed Restricted Three-Body Problem (R3BP), considering shape-based model for the gravity of the two asteroids, when relevant. From on ground observations, a polyhedral model has been made for Didymos, while a tri-axial ellipsoid is assumed for Dimorphos. The highest source of perturbation is the Sun as a fourth body and in the form of Solar Radiation Pressure (SRP). In the time frame of the mission (first half of the year 2027), far from the system (>10 km), the dynamic is dominated by SRP and the Sun gravity field.[6] During close operations, the gravitational attraction of the primary asteroid becomes dominant. Although shape-based models can be used for both asteroids, the irregularities of the gravity field become important only at distances lower than 800 m from the primary.[6] For this reason, in this work, the gravity field of both asteroids will be modelled with a point-mass approach. As a result, the equation of motion for Milani in the quasi-inertial DydimosEclipJ2000 reference frame can be written as

$$\ddot{\mathbf{r}} = -\mu_1 \frac{\mathbf{r_1}}{r_1^3} - \mu_2 \frac{\mathbf{r_2}}{r_2^3} + \mathbf{a_{3body}} + \mathbf{a_{SRP}} \tag{1}$$

Where $\mathbf{r}$ is the CubeSat position, μ_1 and μ_2 are the standard gravitational parameters of the primary and the secondary asteroid, while $\mathbf{r_1}$ and $\mathbf{r_2}$ are their relative position with respect to the considered source of gravity. $\mathbf{a_{3body}}$ is the gravity perturbation of the Sun and it has been simply modelled as

$$\mathbf{a_{3body}} = -\mu_S \left(\frac{\mathbf{r_S}}{r_S^3} - \frac{\mathbf{r_{DS}}}{r_{DS}^3} \right) \tag{2}$$

Where μ_S is the Sun gravity constant, $\mathbf{r_S}$ is the relative position of the third body with respect to the Sun and $\mathbf{r_{DS}}$ is the position of the system with respect to the Sun. Instead, the SRP has been modelled with a cannonball model.[7]

$$\mathbf{a_{SRP}} = \frac{P_0}{c} \left(\frac{d_{SE}}{r_S} \right)^2 \frac{C_r A}{M} \frac{\mathbf{r_S}}{r_S} \tag{3}$$

Where, P_0 (1367 W/m^2) is the solar flux at 1 AU, c is the speed of light, d_{SE} is the Sun-Earth distance (1 AU), C_r is the reflectivity coefficient of the CubeSat, A is its equivalent surface area, and M is the CubeSat mass. The use of the cannonball model highly simplify the mission design since it decouples the orbital dynamics from the spacecraft attitude. To further increase the reliability of the model, a mean value of the reflectivity coefficient and surface area have been used, considering their evolution in time during the mission assuming a reference attitude in an iterative fashion.

MISSION PROFILE

Milani's trajectory design is strongly influenced by the effect of Solar Radiation Pressure (SRP) and the use of a passive payload. The former forbids using stable Keplerian orbits in a low gravity environment, while the latter forces the spacecraft to be always on Didymos' day-side. For these reasons, Milani will hover its target in order to avoid the night-side. Scientific goals and operational constraints have been the main driver for the detailed design of the main phases of Milani's mission: Far Range Phase (FRP) and Close Range Phase (CRP).

Scientific Goals and Operational Constraints

The scientific goals that mostly drove the mission design of Milani involved its main payload, ASPECT.[8] ASPECT is a passive payload, equipped with a visible to near-infrared hypersprectal imager and will be used on Milani to perform global mapping of the asteroids with detailed observations of the DART crater on Dimorphos. ASPECT goals have been translated into several scientific requirements that can be summarized into three main actions:

1. Imaging both the asteroids with a spatial resolution better than 2 m/pixel
2. Imaging the secondary asteroid with a spatial resolution better than 1 m/pixel
3. Imaging the DART crater with a spatial resolution better than 0.5 m/pixel at phase angle (Sun-Asteroid-Milani angle) in the range [0-10] deg and [30-60] deg.

In terms of mission design, spatial resolution requirements drive the ranges at which Milani has to be while performing observations. Among the three ASPECT's channel: Visible (VIS), Near-Infrared (NIR), and Short Wavelength Infrared (SWIR), NIR has the smallest Field Of View (FOV). Thus, the NIR channel drives the maximum ranges at which the observations have to be made.
From an operational point of view, Milani's communication with ground will be performed via Inter-Satellite Link (ISL) using Hera as data relay. For this reason, data downlink and uplink must be performed within the same communication windows used by Hera. Thus, in order to avoid open-loop manoeuvres, Milani needs to manoeuvre with a frequency close to Hera's (4-3 days). It is not mandatory to manoeuver simultaneosly with the mothercraft, however accumulating delay will increase the baseline Turn-Around time (TAT)* of 48 h, so degrading the navigation performances. Instead, manoeuvring ahead of Hera would result in open-loop manoeuvring.

Far Range Phase

FRP has been designed to carry out the mapping of the bodies at a resolution better than 2 m/pixel which translates into being at a distance lower than 11 km from the surface. The absence of any requirements dedicated to specific features on the asteroids lead to simple loop orbits quasi-symmetric with respect to the system. This strategy is simple and has a strong flight heritage around small bodies ensuring also moderate manoeuvre costs. Thus, FRP has been designed as a 6-points hyperbolic loop trajectory as shown in Figure 2 with a manoeuvring pattern of 4-3 days repeated three times. This solution can bring Milani under 9 km of distance from the system to perform the relative observations.

Close Range Phase

CRP has been designed to complete the mapping of Dimorphos at a resolution better than 1 m/pixel and perform the dedicated observation of the DART crater with a resolution better than 0.5 m/pixel. Although mapping at 1 m/pixel requires a range of 5.48 km, the most challenging aspect of this phase is the crater observation that should be performed at a distance at least of 2.78 km from the asteroid. A complex observation of a feature at low range and phase angle on a body in tidally locked configuration, forces the design towards an unusual asymmetric loop as seen in Figure 3. A symmetrical loop similar to the strategy used during FRP is not feasibile, since to get

*TAT is the time between the download of navigation information and the upload of the instruction

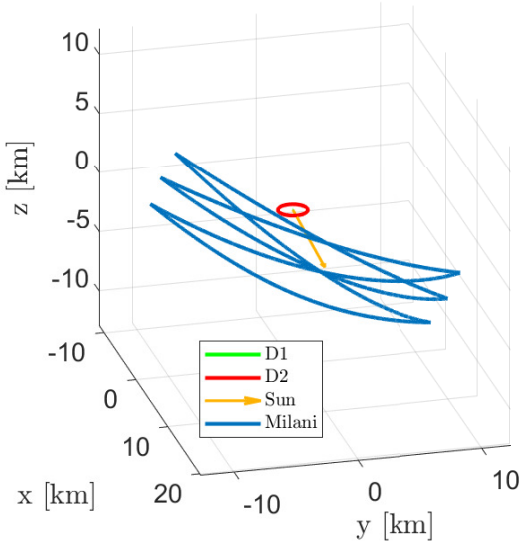

Figure 2. Milani's Far Range Phase (FRP) in the Didymos equatorial Sun South reference frame.

so close to the system a manoeuvring frequency of 1 day would be needed, breaking the operational constraints described before. Furthermore, due to the tidally locked nature of the system, there is a restricted subspace of states in which Milan can imagine the crater in good illumination condition, each period of D2. Hence, Milani needs to phase its motion with the secondary in order to properly image the crater. As a result, differently from FRP design which was focused on the selection of the manoeuvring points, CRP design has focused on the selection of *Key Points* chosen to optimize the close-range observation campaign.

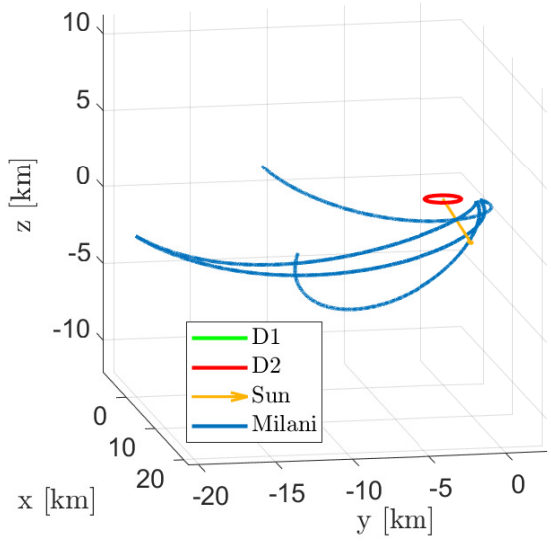

Figure 3. Milani's Close Range Phase (CRP) in the Didymos equatorial Sun South reference frame.

Thus, CRP has been designed as a 4-points loop orbits, 1 pair for each desired range of phase angle. Odd arcs are dedicated to science. During them, Milani is forced to pass through the Key Point, carefully chosen to image the DART impact crater at the desired phase angles and range. Also, the Key Point is phased with Dimorphos at each arc, such that the crater location on the asteroid's surface is found in optimal illumination conditions, at around noon (local time, i.e., when the normal to the surface is towards the Dimorphos-Sun direction). The manoeuvring points of these arcs are positioned after the observations and before the CubeSat goes into Didymos' nightside. Even arcs are recovery trajectories designed to phase the CubeSat with the motion of Dimorphos in order to reach the next Key Point. Moreover, the arc sequence is designed to provide an incremental rotation around the conjunction between Didymos and the Key Point. This process is optimized in terms of manoeuvre cost, as it is designed to leverage the acceleration push of the SRP to change the orbital plane. This is done to shift slowly the orbital plane of each arc towards the terminator plane, to provide a smoother transition to an SSTO, target orbit for the phase following CRP.

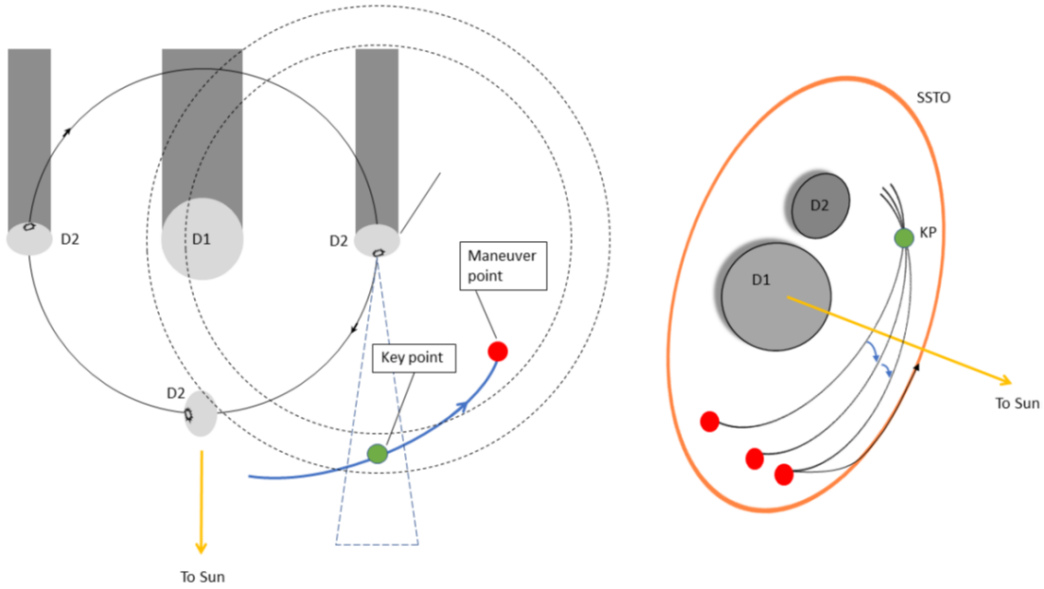

Figure 4. The design framework for CRP trajectories. On the left the choice of the "Key Point" where the CubeSat can image the crater on Dimorphos at optimal illumination conditions, at required distance and phase angle. The odd manoeuvre points are chosen to avoid going into the nightside. On the right the choice of the even manoeuvre points to slowly rotate the orbital plane and facilitate the insertion into the SSTO after the end of the CRP.

The main drawback of the strong asymmetry of this design is to manoeuvre very close to the system with relatively high ΔV. Miniaturized components' performance are not comparable with standard satellites', especially in terms of thrusters' accuracy. As a result, Milani's dispersion would be too high after manoeuvring so close to the system, posing a not negligible safety problem. The solution is to consider long time of flight for these arcs in order to perform correction manoeuvres before arriving to the nominal manoeuvre point. As a result, CRP will adopt a manoeuvring frequency of 7 days allowing for a correction manoeuvre around half the time of flight of the arcs, in order to be compliant with the operational constraints.

NAVIGATION ASSESSMENT

Milani's navigation strategy is based on a combination of optical images, ISL data and LIDAR measurements. The optical images generated by the navigation camera will be processed with landmark-based navigation techniques in order to obtain accurate information about the position of the spacecraft. Since Milani will be released after an initial characterization phase by Hera, it is assumed that a sufficiently detailed shape model will already be available at the beginning of Milani's mission in order to perform navigation tasks. As for the ISL, other than allowing Milani to communicate with Hera, it is also capable of providing measurements of the range and range-rate between the two spacecrafts. This capability will be exploited during the orbit determination process to improve the navigation of the CubeSat. Since the orbit determination of Hera and Milani will be carried out simultaneously, it is possible to rely on a quite accurate knowledge of the mothercraft's position, which makes ISL data beneficial for navigation purposes. Eventually, Milani will carry a LIDAR sensor capable of providing range information with respect to the surface of the asteroids. The maximum operative range of the LIDAR is determined by the albedo of the asteroids. Currently, its value is estimated to be 0.15 ± 0.04,[5] which considering the conservative case leads to an operative range of less than 5500 m for the sensor. Therefore, it will be employed only for limited parts of the mission.

The orbit determination process will be carried out at ESA's European Space Operations Centre (ESOC). Operational constraints set by ESA led to the definition of a 48 hours TAT, which has become a key factor for the assessment of the navigation performance. The TAT is the time between the downlink of the navigation information on ground and the uplink of the next set of instructions to the spacecraft. Thus, a longer TAT will inevitably degrade the navigation performance, since it limits the amount of data that can be gathered and used for the orbit determination process. Additionally, a time margin between the uplink of the instruction set and the execution of the following manoeuvre has been considered. During FRP this margin is set to 1 hour for all arcs, in order to allow a sufficient amount of time for the correct execution of the instructions. During CRP, instead, the time margin changes slightly between different arcs, in order to keep the desired phasing with Dimorphos. However, it is always set greater or equal than 1 hour. Thus, the last navigation measurement can actually be taken 49 hours before the end of the arc, at best. The time instant that marks the last possible measurement to be used before the next manoeuvre is called Cutoff time (COT). Measurements taken before COT are sent to ground and are used for the orbit determination of the current trajectory arc. After COT, navigation measurements can still be generated, but they cannot be used for the orbit determination of the current arc. Instead, they can be employed together with data generated during the next trajectory arc, in order to improve the orbit determination by decreasing a-posteriori the uncertainty in correspondence of the manoeuvre.
Milani's operational concept is illustrated in Figure 5. In the current strategy, the only navigation data generated after each arc's COT are a set of optical images to be processed during the following trajectory arc.

Covariance Analysis

A covariance analysis has been performed on the nominal trajectory to assess the state knowledge that can be achieved with the available information. The knowledge represents the difference between the estimated trajectory and the real one. An Extended Kalman Filter (EKF) is employed to estimate the state of the spacecraft. For each mission phase, the filter is initialized considering the knowledge at the end of the previous phase, to which the additional uncertainty given by ma-

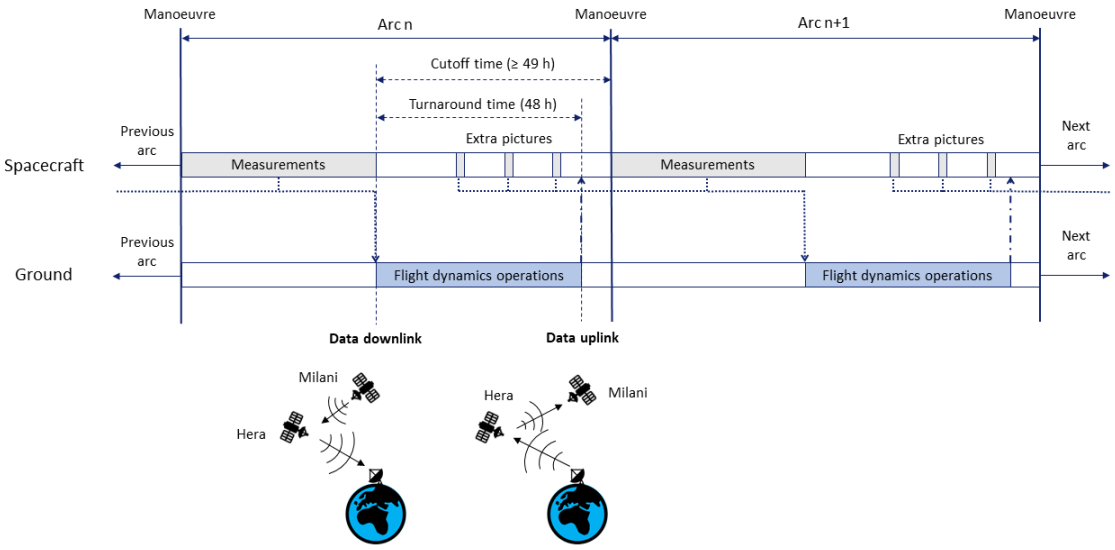

Figure 5. Assumed operations timeline for the Milani mission.

noeuvres is added. In particular, for each manoeuvre a 1% magnitude error and a 1 degree angle error in each direction (1-sigma) have been considered.
The Kalman filter equations are summarized in Equations (4)–(8).

$$\delta\bar{\mathbf{x}}_\mathbf{k} = \Phi(t_k, t_{k-1})\delta\hat{\mathbf{x}}_{\mathbf{k-1}} \tag{4}$$

$$\bar{\mathbf{P}}_\mathbf{k} = \Phi(t_k, t_{k-1})\mathbf{P}_{\mathbf{k-1}}\Phi^{\mathrm{T}}(t_k, t_{k-1}) + \int_{t_{k-1}}^{t_k} \Phi(t_k, \tau)\mathbf{B}\mathbf{Q}\mathbf{B}^{\mathrm{T}}\Phi^{\mathrm{T}}(t_k, \tau)d\tau \tag{5}$$

$$\mathbf{K}_\mathbf{k} = \bar{\mathbf{P}}_\mathbf{k}\mathbf{H}_\mathbf{k}^{\mathrm{T}}\left(\mathbf{H}_\mathbf{k}\bar{\mathbf{P}}_\mathbf{k}\mathbf{H}_\mathbf{k}^{\mathrm{T}} + \mathbf{R}\right)^{-1} \tag{6}$$

$$\mathbf{P}_\mathbf{k} = (\mathbf{I} - \mathbf{K}_\mathbf{k}\mathbf{H}_\mathbf{k})\bar{\mathbf{P}}_\mathbf{k}(\mathbf{I} - \mathbf{K}_\mathbf{k}\mathbf{H}_\mathbf{k})^{\mathrm{T}} + \mathbf{K}_\mathbf{k}\mathbf{R}\mathbf{K}_\mathbf{k}^{\mathrm{T}} \tag{7}$$

$$\delta\hat{\mathbf{x}}_\mathbf{k} = \delta\bar{\mathbf{x}}_\mathbf{k} + \mathbf{K}_\mathbf{k}(\mathbf{y} - \mathbf{H}_\mathbf{k}\delta\bar{\mathbf{x}}_\mathbf{k}) \tag{8}$$

where $\delta\mathbf{x}_\mathbf{k}$ is the deviation from the nominal state, $\Phi(t_k, t_{k-1})$ is the state transition matrix (STM) from t_{k-1} to t_k, $\mathbf{P}$ is the covariance matrix of the state, $\mathbf{B}$ is a matrix mapping noise elements to state elements, $\mathbf{Q}$ is the process noise covariance matrix, $\mathbf{K}$ is the Kalman gain, $\mathbf{H}$ is the Jacobian of the measurements model with respect to the state, $\mathbf{R}$ is the covariance matrix of the measurements, $\mathbf{I}$ is the identity matrix and $\mathbf{y}$ is the measurement vector. Equation 7 is the Joseph form of the covariance update, which is known to be more numerically stable than the original Kalman form.[9]
Process noise is introduced to account for residual accelerations and Solar Radiation Pressure (SRP) variability (SRP is modelled as deterministic, but with a stochastic fraction). Both are modelled as first order Gauss–Markov (GM) processes, thus they are included in the state vector, giving a total of 12 estimated state elements: 6 for the spacecraft position and velocity, 3 for the residual acceleration and 3 for the SRP's stochastic part. To account for the additional state variables, the STM has been augmented with the approach outlined by Tapley.[10]

The properties assumed for the GM processes are reported in Table 2.

Table 2. Gauss–Markov processes properties

	σ	τ
Residual acceleration	$5 \times 10^{-9} m/s^2$	1 day
Solar Radiation Pressure	8% of SRP acceleration	1 day

Pseudo-measurements generation Milani's navigation has been simulated considering radiometric measurements from the ISL, optical landmarks observation and LIDAR measurements. In this section the model used for each of the observables is described, starting with the optical navigation.

In order to obtain a realistic assessment of the spacecraft's navigation performance, a surrogate model for the generation of the landmark observations has been developed. It employs a flat-surface shape model of D1, where some faces are randomly selected as "hosting" a landmark. The line-of-sight (LOS) from the satellite to the centre of each of these faces represents an observable. To exclude features that would not be visible from the spacecraft, the selected surfaces are pruned by considering the relative position, the navigation camera's field of view (FOV) and the Phase Angle. This ensures that features on the far-side of the asteroid, outside of the FOV, and/or not illuminated are not considered for navigation purposes. An example of the output of the model is illustrated in Figure 6, where the LOS from the spacecraft to the visible features on the shape model are shown. In the navigation analysis 100 total features have been generated on the shape model.

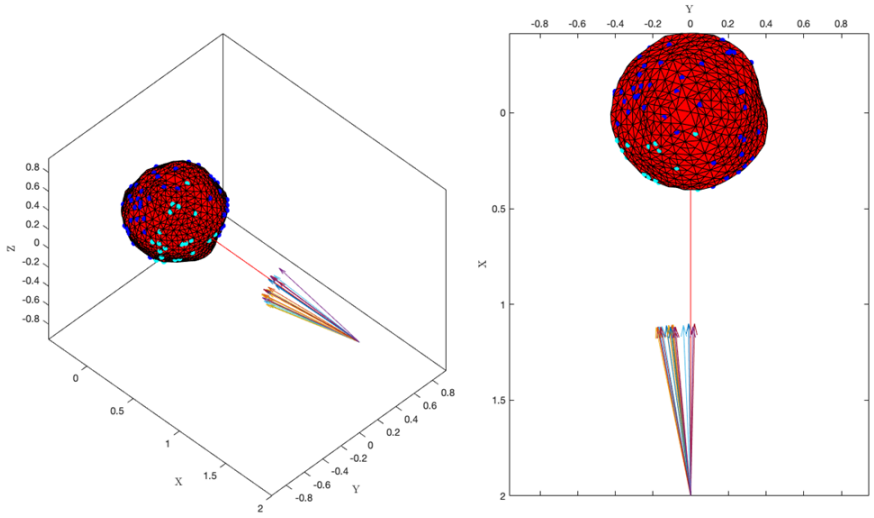

Figure 6. Output of the optical navigation surrogate model. The randomly generated features are shown on the shape model of the asteroid, and the visible features are highlighted. The LOS from the spacecraft to the visible features are also shown. Left: 3D view. Right: View of the XY plane from above.

After the ideal LOS is generated from the surrogate model, an angular error is added according to

the measurement error covariance. The filter selects a subset of the available LOS, and then treats each of them as a separate measurement for the update. The derivative of the LOS with respect to the state is given by

$$\mathbf{H_{LOS}} = \left[\frac{\partial \mathbf{y_{LOS}}}{\partial \mathbf{x}}\right] = \left[-\left(\frac{\mathbf{I}}{||\mathbf{p}||} - \frac{\mathbf{p}\mathbf{p}^{\mathrm{T}}}{||\mathbf{p}||^3}\right) \quad \mathbf{0_{3\times 9}}\right] \tag{9}$$

where $\mathbf{p}$ is the vector from the spacecraft to the selected feature and $\mathbf{0_{3\times 9}}$ is a 3×9 matrix of zeros, given by the fact that the measurement depends only on the position of the spacecraft, thus the derivatives with respect to the other state elements are all zero.
The measurement error on the LOS direction is generated by converting the LOS to spherical coordinates and then introducing an error on the azimuth and elevation angles. The error is assumed to be independent on each angle, with standard deviation given by

$$\sigma_\varepsilon = \sqrt{\sigma_{IP}^2 + \sigma_{point}^2} \tag{10}$$

where σ_{IP} is the contribution due to image processing errors, while σ_{point} accounts for camera alignment uncertainty. The LOS is then converted back to cartesian coordinates, and the same is also done for the covariance matrix. They are then employed in the filter for the measurement update.
As for ISL measurements, the range and range-rate with respect to Hera are given by

$$\rho = \sqrt{(\mathbf{p_M} - \mathbf{p_H})(\mathbf{p_M} - \mathbf{p_H})^{\mathrm{T}}} \tag{11}$$

$$\dot{\rho} = \frac{(\mathbf{p_M} - \mathbf{p_H})(\mathbf{v_M} - \mathbf{v_H})^{\mathrm{T}}}{\rho} \tag{12}$$

where ρ is the range, $\dot{\rho}$ is the range-rate and $\mathbf{p_M}$ and $\mathbf{p_H}$, $\mathbf{v_M}$ and $\mathbf{v_H}$ are respectively the position and velocity of Milani and Hera. Their Jacobian is given by

$$\mathbf{H}_\rho = \left[\frac{\partial \rho}{\partial \mathbf{x}}\right] = \left[\frac{(\mathbf{p_M}-\mathbf{p_H})^{\mathrm{T}}}{\rho} \quad \mathbf{0_{1\times 9}}\right] \tag{13}$$

$$\mathbf{H}_{\dot{\rho}} = \left[\frac{\partial \dot{\rho}}{\partial \mathbf{x}}\right] = \left[\frac{(\mathbf{v_M}-\mathbf{v_H})^{\mathrm{T}}}{\rho} - \frac{(\mathbf{p_M}-\mathbf{p_H})^{\mathrm{T}}\dot{\rho}}{\rho^2} \quad \frac{(\mathbf{p_M}-\mathbf{p_H})^{\mathrm{T}}}{\rho} \quad \mathbf{0_{1\times 6}}\right] \tag{14}$$

The range and range-rate errors also account for two contributions: one is due to the ISL measurement error, while the other accounts for the uncertainty in the knowledge of Hera's state. Thus, their standard deviation is given by

$$\sigma_\rho = \sqrt{\sigma_{ISL_\rho}^2 + \sigma_{H_p}^2} \tag{15}$$

$$\sigma_{\dot{\rho}} = \sqrt{\sigma_{ISL_{\dot{\rho}}}^2 + \sigma_{H_v}^2} \tag{16}$$

where σ_{H_p} and σ_{H_v} are the uncertainties on Hera's position and velocity, respectively.
The equations for the LIDAR measurement are given by

$$y_L = \left|\left|\mathbf{p_{rel}} - r_{D1}\frac{\mathbf{p_{rel}}}{||\mathbf{p_{rel}}||}\right|\right| \tag{17}$$

$$\mathbf{H_L} = \left[\frac{\partial y_L}{\partial \mathbf{x}}\right] = \left[\frac{\left(\mathbf{p_{rel}} - r_{D1}\frac{\mathbf{p_{rel}}}{||\mathbf{p_{rel}}||}\right)^{\mathrm{T}}}{y_L} \quad \mathbf{0_{1\times 9}}\right] \tag{18}$$

where $\mathbf{p_{rel}}$ is the relative position of the spacecraft with respect to Didymos and r_{D1} is Didymos' radius. Equations (17) and (18) assume a spherical surface for the main body. Thus, to account for modelling errors deriving from this assumption, the error associated to LIDAR measurements has been increased:

$$\sigma_L = \sqrt{\sigma_s^2 + \sigma_{D1}^2} \tag{19}$$

in which σ_s is the error due to the LIDAR sensor, while σ_{D1}^2 is the contribution do to the shape of Didymos.
The values employed for the measurement uncertainties are reported in Table 3.

Table 3. Measurements uncertainty values

Parameter	Value
σ_{IP}	1 IFOV = 37.2 arcsec
σ_{point}	90 arcsec
σ_{ISL_ρ}	0.5 m
σ_{H_p}	10 m
$\sigma_{ISL_{\dot{\rho}}}$	1.5 cm/s
σ_{H_v}	1 cm/s
σ_s	1 m
σ_{D1}	10 m

Results In this section the results of the analysis are presented. Measurements are generated according to the following assumptions:

- 7 navigation images are generated on each trajectory arc, 4 of which before the COT and 3 after.
- ISL measurements start 6 hours after the beginning of each arc and end 3 hours before the COT. Range measurements are taken every 3 hours, while range-rate measurements every hour.
- When the LIDAR is within its operative range, its measurements are taken every 3 hours, starting 1 hour after the beginning of the arc and end 1 hour before the COT.

Results are presented in the EclipJ2000 frame. Figures 7 and 8 show the position and velocity standard deviations predicted by the filter during FRP. In particular, the square roots of the diagonal elements of the covariance matrix are shown. The total knowledge, represented in black, is obtained as the root sum squared of the diagonal elements. Manoeuvres, optical navigation images and cutoff times are shown with dashed vertical lines, while ISL measurement windows are highlighted in grey. Finally, the total standard deviation obtained only with measurements taken before the COT is shown with a black dot-dashed line.
Optical navigation gives the highest contribution to the spacecraft knowledge. Indeed, landmark-based navigation allows an accurate estimation of its position, which also leads to improved velocity knowledge thanks to the filtering algorithm. The ISL's contribution is limited, but not negligible. It depends strongly on the relative position and velocity of Milani and Hera, which change slowly in time due to the low velocity of the spacecrafts relative to the asteroid system. Furthermore,

the uncertainty on Hera's state further degrades the ISL performance. However, range and range-rate measurements help keeping the total standard deviation below 100 m during most of the FRP. Results are satisfactory also for the velocity knowledge, which is below 1 mm/s during most of the trajectory, except shortly after manoeuvres.

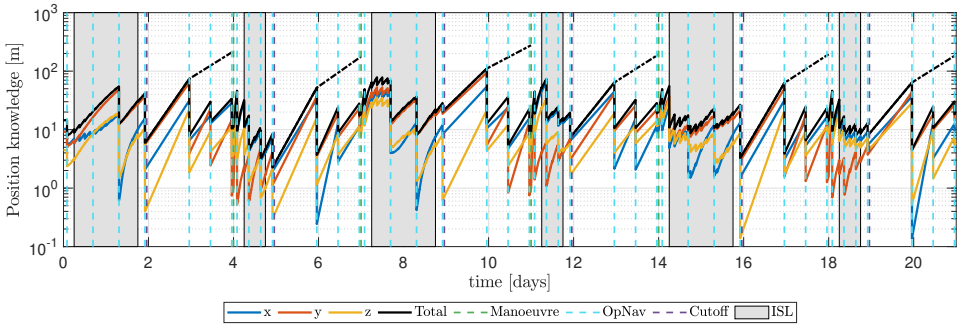

Figure 7. Covariance of position error during FRP.

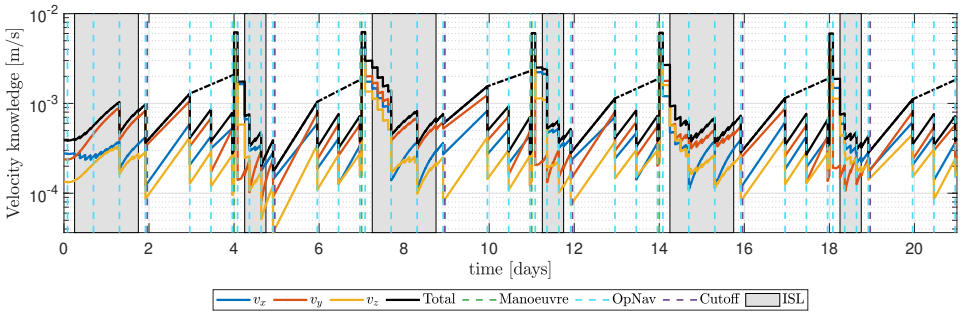

Figure 8. Covariance of velocity error during FRP.

CRP results are presented in Figures 9 and 10. Note that in this phase some of the manoeuvres are purely correction manoeuvres, which do not have a deterministic ΔV. Therefore, in such cases there is not a corresponding jump in the velocity uncertainty. It can be clearly noticed that during CRP the performance of the optical navigation images change significantly, which is due to the great variations of the range with respect to Didymos. Indeed, the closer the spacecraft is to the system, the better the optical navigation performance. However, thanks to the combination of ISL and optical navigation, also in this case the position and velocity knowledge remain below 100 m and 1 mm/s, respectively, for most of the CRP.

CONCLUSIONS

This paper discusses the main challenges and solutions for the trajectory design and navigation of the Milani mission. The complexity of orbiting in a highly perturbed low-gravity environment is increased by the use of miniaturized components and by the navigation constraints of an opportunity payload. In particular, the constraint on the manoeuvring frequency has the strongest impact, since

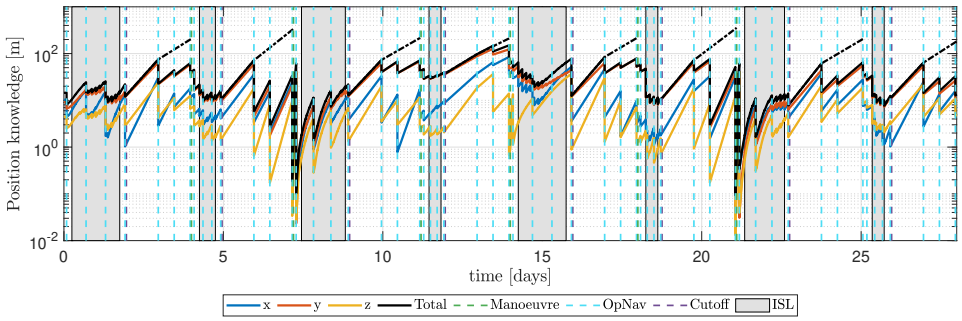

Figure 9. Covariance of position error during CRP.

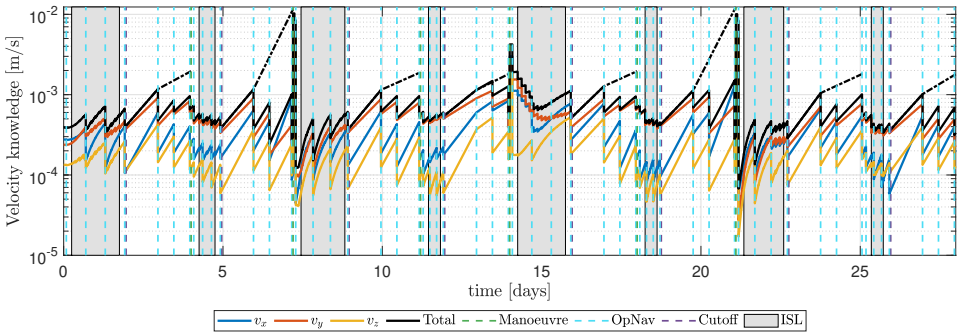

Figure 10. Covariance of velocity error during CRP.

the range of possible altitudes reached while hovering a small body strongly depends on the time of flight of the ballistic arcs. The solutions presented clearly show how the design gets more complex when the CubeSat needs to get closer to the system. The Far Range Phase requirements can be met with symmetric loop orbits and a relaxed manoeuvring pattern of 4 and 3 days. On the other hand, during Close Range Phase the spacecraft must get very close to Dimorphos. Thus, it requires a complex asymmetric design with the definition of keypoints at which Milani can perform science and a concurrent phasing with the motion of Dimorphos and the manoeuvring schedule of Hera. The strong asymmetry is also due to the need of performing correction manoeuvres in order to deal with the inaccuracies given by thruster errors.
Milani's navigation is also not trivial. The 48 h constraint on the TAT and the relatively high perturbations of the dynamics lead to the need of performing measurements also after the COT to reduce the uncertainty. With the proposed strategy, Milani could navigate with a knowledge in the order of tens of metres for the most part of the mission.

ACKNOWLEDGEMENT

This work has been performed under Tyvak International contract within the scope of ESA Contract No. 1222343567/62/NL/GLC. The authors would like to acknowledge the support received by the whole Milani Consortium.

REFERENCES

[1] A. Cheng, J. Atchison, B. Kantsiper, A. Rivkin, A. Stickle, C. Reed, A. Galvez, I. Carnelli, P. Michel, and S. Ulamec, "Asteroid Impact and Deflection Assessment mission," *Acta Astronautica*, Vol. 115, 2015, pp. 262–269.

[2] A. F. Cheng, A. S. Rivkin, P. Michel, J. Atchison, O. Barnouin, L. Benner, N. L. Chabot, C. Ernst, E. G. Fahnestock, M. Kueppers, P. Pravec, E. Rainey, D. C. Richardson, A. M. Stickle, and C. Thomas, "AIDA DART asteroid deflection test: Planetary defense and science objectives," *Planetary and Space Science*, Vol. 157, 2018, pp. 104–115.

[3] F. Ferrari, V. Franzese, M. Pugliatti, C. Giordano, and F. Topputo, "Preliminary mission profile of Hera's Milani CubeSat," *Advances in Space Research*, Vol. 67, No. 6, 2021, pp. 2010–2029.

[4] O. Karatekin, H. Goldberg, C.-L. Prioroc, and V. Villa, "Juventas: Exploration of a binary asteroid system with a cubesat.," *Proceedings of the International Astronautical Congress, IAC*, Vol. 2019-October, 2019.

[5] S. Naidu, L. Benner, M. Brozovic, M. Nolan, S. Ostro, J. Margot, J. Giorgini, T. Hirabayashi, D. Scheeres, P. Pravec, P. Scheirich, C. Magri, and J. Jao, "Radar observations and a physical model of binary near-Earth asteroid 65803 Didymos, target of the DART mission," *Icarus*, Vol. 348, 2020, p. 113777.

[6] F. Ferrari, V. Franzese, M. Pugliatti, C. Giordano, and F. Topputo, "Trajectory options for Hera's Milani CubeSat around (65803) Didymos," *The Journal of the Astronautical Science, submitted*, 2021.

[7] I. Jean, A. Ng, and A. K. Misra, "Impact of solar radiation pressure modeling on orbital dynamics in the vicinity of binary asteroids," *Acta Astronautica*, Vol. 165, 2019, pp. 167–183.

[8] T. Kohout, A. Näsilä, T. Tikka, M. Granvik, A. Kestilä, A. Penttilä, J. Kuhno, K. Muinonen, K. Viherkanto, and E. Kallio, "Feasibility of asteroid exploration using CubeSats—ASPECT case study," *Advances in Space Research*, Vol. 62, No. 8, 2018, pp. 2239–2244.

[9] D. Simon, *Optimal State Estimation: Kalman, H Infinity, And Nonlinear Approaches*. Wiley, 2006.

[10] B. D. Tapley, B. E. Schutz, and G. H. Born, *Statistical Orbit Determination*. Elsevier, 2004.